A facile strategy to determine photon flux and effective optical path length in intensified continuous-flow photoreactors

Stefan D.A. Zondag,[1],† Jasper H.A. Schuurmans,[1],† Arnab Chaudhuri,[2],† Robin P.L. Visser,[2] Cíntia Soares,[3] Natan Padoin,[3] Koen P.L. Kuijpers,[4] Matthieu Dorbec,[4] John van der Schaaf,[2],* Timothy Noël[1],*

[1] Flow Chemistry Group, van't Hoff Institute for Molecular Sciences (HIMS), Universiteit van Amsterdam (UvA), 1098 XH Amsterdam, The Netherlands.

[2] Department of Chemical Engineering and Chemistry, Sustainable Process Engineering, Eindhoven University of Technology (TU/e), 5612 AZ Eindhoven, The Netherlands.

[3] Department of Chemical and Food Engineering, Federal University of Santa Catarina, Florianópolis/SC, 88040-900, Brazil.

[4] Technology and Engineering Group, Janssen Research and Development, Turnhoutseweg 30, 2340 Beerse, Belgium.

† These authors contributed equally to the work.

* Corresponding Author(s): t.noel@uva.nl (Timothy Noël) and j.vanderschaaf@tue.nl (John van der Schaaf)

Abstract

Photocatalysis for small molecule activation has seen significant advancements over the past decade, yet its scale-up remains a challenge due to photon attenuation effects. A promising solution lies in harnessing high photonic intensities paired with continuous-flow reactor technology. However, a deep grasp of photon transport is essential, typically demanding resource-intensive experiments. To address this, we introduce an innovative approach to photochemical reactor setup characterization, starting with radiometric light source analysis and progressing to a 3D reactor simulation for photon flux determination. Contrary to conventional techniques that prioritize complete photon absorption, our technique operates optimally when the reaction mixture is unsaturated. This strategy decouples photon flux and path length determination, substantially curtailing the experimental process. The workflow proves versatile across various reactor systems, simplifying intricate light interactions into a single one-dimensional parameter, i.e., the effective optical path length. Combined with the photon flux, this parameter effectively characterizes photochemical setups, irrespective of scale, geometry, light intensity, or photocatalyst concentration. Employing radiometry further offers insights into light source positioning and reactor design, and obviates the need for repeated chemical actinometry measurements due to light source degradation. Additionally, the proposed workflow facilitates experiments at lower concentrations, ensuring optimal reactor operation. In essence, our approach provides a thorough, efficient, and consistent framework for reactor irradiation characterization.

Keywords: Process intensification - photochemistry - reactor characterization - chemical actinometry - radiometry - photon flux - optical path length

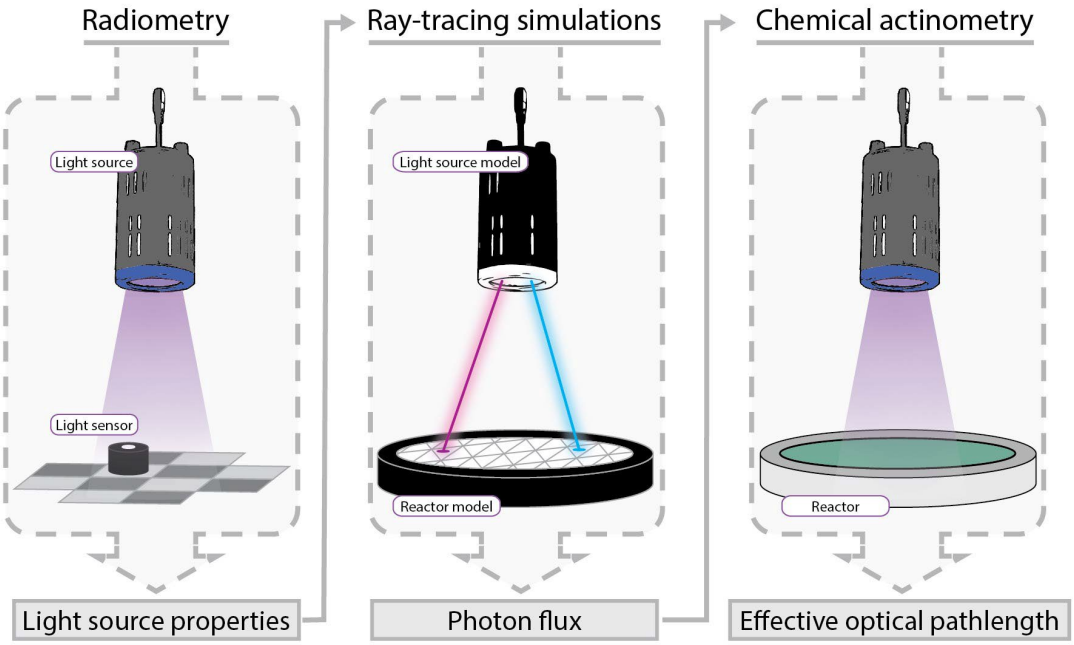

Introduction

Photons play a pivotal role in modern synthetic chemistry, particularly in the activation of small organic molecules using photocatalysis.[1] Their use has the potential to alter the landscape of chemical processes, ushering in an era of greener and more sustainable methodologies. Of particular interest to the synthesis of pharmaceuticals and agrochemicals is that these reactions often unfold under remarkably benign conditions, such as ambient temperature and visible light.[2–4] While photocatalysis is well-integrated on a smaller scale, such as in medicinal chemistry, its upscaling often presents significant challenges.[5–7] Firstly, the sheer volume of photons required for large-scale photocatalytic transformations necessitates several kW of optical power to produce compounds in substantial quantities. Secondly, the attenuation of light as it travels through the reactor diminishes its intensity, leading to undesirable variations in kinetic rates which can, in turn, trigger byproduct formation. Given these complexities, there is an evident demand for precise modeling and straightforward characterization of photochemical reactor technology, providing essential guidance for chemical process engineers.

Successful design of photochemical processes hinges on two key factors: identifying the number of absorbed photons and deciphering its correlation to the production of the desired compound.[8] The former encompasses the irradiation profile within the reactor, where the average path length of photons emerges as a pivotal element. The latter revolves around the quantum yield, a metric that enumerates reactive events per absorbed photon.[9,10] Traditionally, chemical actinometry studies have been the predominant strategy to generate this wealth of information.[11] Yet, the experimental conditions demanded by actinometric measurements pose challenges.[12,13] Further complicating matters, the inherent variability in light intensity over a light source's lifespan necessitates laborious recalibrations through actinometry.

In our pursuit to further improve the scalability of photocatalytic processes, we introduce a streamlined workflow that separates the determination of photon flux from traditional actinometry experiments. Our method relies on radiometry to capture data regarding the light intensity of employed light sources. Leveraging this data, a light source model is formulated, which then facilitates the simulation of the maximal photon flux reaching the reaction mixture. This simulation employs ray-tracing,[14–16] taking into account the reactor's material composition and geometric design. Armed with this insight, the experimental outcomes of chemical actinometry are repurposed to discern the effective optical path length rather than the photon flux. This pivot alleviates constraints on the absorbance in actinometry experiments, simplifying data collection by enabling exploration of extended irradiation durations or diminished concentrations. To showcase its efficacy, our method was validated on a non-intensified batch setup and subsequently applied to two distinct intensified flow reactors; a capillary reactor and a rotor-stator spinning disk reactor. Benchmark tests underscored the method's remarkable accuracy coupled with reduced effort post-model formulation. With the burgeoning interest in photocatalysis within industrial spheres, we posit that our approach is paramount for a nuanced comprehension of vital photochemical processes, paving the way for seamless scale-ups from lab to pilot and eventually, commercial levels. Additionally, our strategy offers a deeper dive into the energy balance of photochemical reactions, a crucial component for future operational expense (OPEX) analyses of the entire process.[17]

Limitations of chemical actinometry for intensified photochemical reactor platforms

Chemical actinometry has long served as a cornerstone technique for determining quantum yield and photon flux in photochemical processes. While it has proven invaluable in many traditional settings, its applicability and accuracy come into question when we transition to photochemical reactor platforms with highly transmitting characteristics.[18] These advanced reactor systems, designed for enhanced efficiency and throughput, introduce a set of complexities that can challenge the conventional actinometric methods. In this subsection, we discuss the specific limitations and constraints of

employing chemical actinometry in such intensified settings, underscoring the need for innovative approaches to reactor characterization.

The quantum yield plays a pivotal role in the mechanistic exploration of photochemical reactions. It stands as a primary determinant of requisite photon equivalents.[8] This parameter offers insights into the reaction mechanism, such as chain reactions, and gauges the efficiency of the photochemical process.[19–22] As such, ensuring the precision of the quantum yield becomes imperative. This necessitates knowledge of the system's photon flux (expressed in mol s^{-1}, or commonly as E s^{-1}, where Einstein represents a mole of photons).[23] Chemical actinometry emerges as the conventional method for acquiring this data. Specifically, actinometry leverages reactions with established quantum yields to experimentally deduce the photon flux,[24] guided by the Bouguer-Lambert-Beer law (Equation 1). This law describes the transmittance of light (T) as a change in light intensity (I) against its initial value (I_0), due to the absorbance (A) within a uniform, isotropic medium. The absorbance escalates rapidly when light traverses a known distance (l) through an attenuating medium that is characterized by the concentration of the absorbing species (C) and its (decadic) molar attenuation coefficient (ε).

For any given (photo)chemical system, a molar balance can be derived, as illustrated in Equation 2 using an exemplary chemical actinometry batch experiment under ideal conditions.[18,25] In this context, the rate at which the number of moles of species i changes over time (dN_i/dt) is governed by the photon flux reaching the medium ($q_{n,p}$). This is further influenced by the light absorbed by the attenuating species i, represented as the fraction of light that the system does not transmit ($1 - T$), and the known quantum yield of the reaction (φ).

$$T = \frac{I}{I_0} = 10^{-A} = 10^{-\varepsilon C l} \tag{1}$$

$$\frac{dN_i}{dt} = -\varphi q_{n,p}(1 - T) = -\varphi q_{n,p}(1 - 10^{-\varepsilon_i C_i l}) \tag{2}$$

In photochemical reactions, not every emitted photon by the light source interacts with the reaction mixture. Factors such as the positioning of the reactor relative to the light source, reflection losses, and other material interferences play a role. Those photons that do penetrate the reaction mixture contribute to the initial intensity (I_0), defined at the inner surface of the reactor. This is the boundary where the reactor material meets the reaction mixture. Subsequently, the decline in light intensity within the reaction mixture is governed by the concentration of the attenuating species and its molar attenuation coefficient. It is also influenced by the distance the light covers within the medium. This distance, termed the optical path length, serves as an average descriptor of the setup's layout, and is independent of the absorbing species properties.

It is essential to clarify that the absorbance term for a single-phase system, represented by $A = \varepsilon_i C_i l$, can ideally be divided into two distinct components. The first component is influenced by the attenuation properties of the species within the homogeneous medium, denoted by $\varepsilon_i C_i$. The second, the path length l, is exclusively affected by the configuration of the reactor and light source. In scenarios with high concentrations, potent absorbing species, or extended path lengths, most of the photons are absorbed. This leads to pronounced absorbance values and, consequently, minimal transmittance. As a result, the fraction of light diminished by the system (represented by the $1 - T$ term in Equation 2) approaches unity, implying the reactor absorbs virtually all incoming light. This scenario streamlines

the molar balance, rendering the precise depiction of the optical path length in the system redundant. Hence, variations in this path length would have negligible repercussions on the overall molar balance.[i]

Another prevalent simplification in determining the photon flux hinges on the presumption of a linear rate of change. Typically, this is achieved by conducting experiments over brief irradiation durations, ensuring minimal chemical conversion. With the understanding that a system with low chemical conversions almost entirely absorbs incoming light, Equation 2 can be further simplified to deduce the photon flux, as illustrated in Equation 3.

$$q_{n,p} \approx -\frac{\Delta N_i}{\Delta t\ \varphi} \tag{3}$$

In recent times, there has been a shift towards conducting photochemical reactions in intensified photoreactors. These reactors combine short path lengths with potent light sources, aiming to amplify productivity and selectivity via uniform irradiation profiles and increased photon intensities.[26,27] Such intensified systems are at the forefront of sustainable and reliable photochemical scale-ups, attracting considerable interest from both industry and academia.[28,29] Some prominent reactor examples include microcapillary reactors, vortex type and oscillatory reactors.[30–34] However, a crucial aspect to underscore here is that these short path length reactors often do not absorb all photons in a single pass. As a result, photons can effectively leave the system, leading to a scenario where the system does not achieve complete absorption (i.e., $T \neq 0$), as illustrated in Figure 1. To compensate for these unabsorbed photons, a precise measure of the optical path length becomes essential. This measurement is especially critical when the system's attenuation features vary, such as when determining the quantum yield for different photochemical reactions using an identical setup (see Supplementary Information). Within this context, a photon-efficient photoreactor can be primarily defined by its relatively long effective path length. And interestingly, as the Bouguer-Lambert-Beer law only portrays relative intensity, this classification remains somewhat detached from the employed optical power. It is worth noting, however, that with high-power light sources, the system's attenuation properties (like the concentration of absorbing entities) can undergo rapid alterations. High chemical conversions achieved within short irradiation times can transform a setup into a non-photon-efficient one, causing the light transmission to transition from nearly zero to a notable fraction in a short time span.

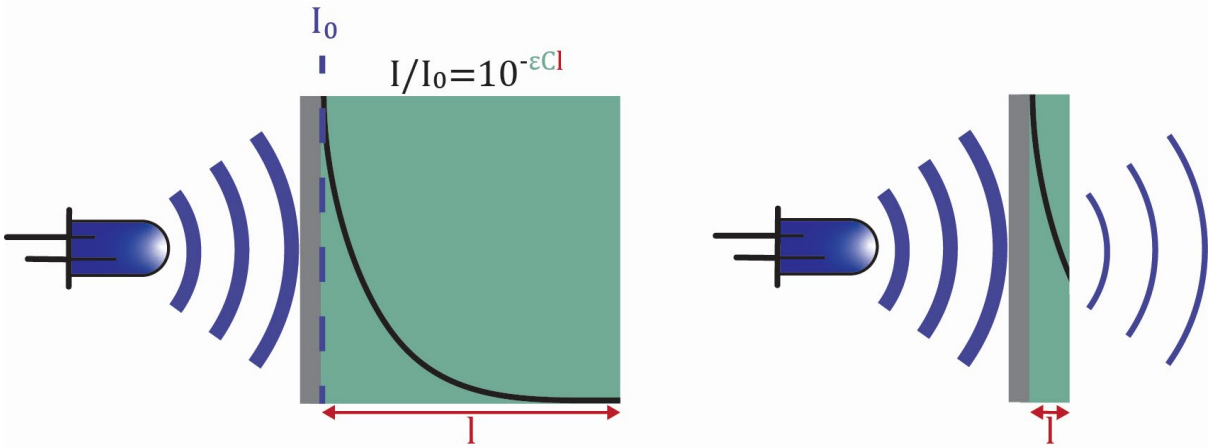

Figure 1. Visualization of the light intensity in a photon-efficient system (left) and non-photon-efficient system (right), illustrating the Bouguer-Lambert-Beer law, as given in equation (1). Here, the main difference is the residual intensity transmitted after travelling the path length l through the attenuating medium.

[i] An important distinction to make is the one between the penetration depth, which is defined as the distance where the transmittance is equal to $e^{-1} \approx 0.37$, and the optical path length, which is the distance travelled by light within a medium, given that its intensity never fully attenuates.

While strides have been made in discerning the photon flux in intensified reactors, challenges remain. Various methods have been proposed to sustain high absorbance (meaning low actinometer conversion) and prevent product precipitation – these include shortening irradiation times or introducing pulsation.[35,36] Yet, inaccuracies in path length can still profoundly skew the photon flux measurements in intensified systems. Deriving the path length purely based on geometry, such as using reactor diameter or other geometrical approximations, is not always reliable. This is because light sources come with unique emission distribution patterns, and factors like refraction, back reflection, and total internal reflection can alter the effective optical path length.[13,18,37] While spectro-radiometric measurements offer a way to delineate the system's path length,[38,39] their precision can be compromised in scenarios with uneven irradiation fields or when bulky light sensors are paired with micro-scaled (or intensified) reactors.[40] Furthermore, achieving accuracy becomes more challenging when interfaces of materials, each having distinct refractive indices, affect the local irradiation profile.

In light of the challenges presented, we introduce a method that seamlessly decouples photon flux from path length determination, eliminating the need for laborious and repetitive experimental work. Our versatile approach, adaptable across a range of systems, simplifies intricate light interactions into a singular, one-dimensional parameter: the effective optical path length. This systematic approach not only streamlines reactor characterization but also enhances the accuracy and reproducibility of photochemical processes.

Results and discussion

In this study, we utilized the widely recognized potassium ferrioxalate actinometer (Reaction 1),[11,20,41,42] of which the quantum yield has been explored across an extensive wavelength range.[43] We employed several pseudo-monochromatic UV-A LED light sources, and their spectral distributions were determined using a spectrophotometer (Supplementary Figure S4a). The decadic molar attenuation coefficients for the potassium ferrioxalate complex and its subsequent products were measured for relevant wavelengths within the emission spectra (Supplementary Figure S8a). An important conclusion from these measurements is the minimal attenuation coefficient of the resultant products compared to the initial material. This underscores the potassium ferrioxalate complex as the principal absorbing species, simplifying the absorbance assessment.

1 $$2[Fe(III)(C_2O_4)_3]^{3-} \xrightarrow{h\nu} 2[Fe(II)(C_2O_4)_2]^{2-} + 2CO_2 + C_2O_4^{2-}$$

A) Non-intensified photochemical batch reactor

In assessing highly photon transmitting systems, understanding the effective optical path length is essential. However, as a preliminary step in our proposed method, we sought to underscore its limited significance in a photon-efficient context. Our initial experiments, therefore, targeted a basic setup anticipated to have a sufficiently long effective optical path length. Hereto, we employed a batch configuration, which consisted of a test tube (13 mm inner diameter, 15 mm outer diameter) filled with the reaction mixture and illuminated by a high-powered LED light source. This off-the-shelf lamp offers four distinct power settings, enabling us to evaluate the same batch setup across four separate data sets. Instead of the conventional chemical actinometry approach to assess the photon flux absorbed by the reaction mixture, we used a combination of radiometric measurements, 3D modeling, and ray-tracing simulations. Fundamentally, our methodology zeroes in on an exhaustive characterization of the light source, harnessing this data to fine-tune a corresponding model, and subsequently applying this model to a virtual rendition of the experimental setup.

We initiated our study with radiometric measurements, utilizing a calibrated light sensor strategically positioned within a pre-established grid. This setup facilitated the precise mapping of light intensity across an irradiated plane. Using the physical dimensions of the light source, we crafted a 3D model and simulated the radiometric conditions using ray-tracing within the COMSOL Optics Module (detailed in the Supplementary Information). This virtual model of the light source was complemented by an accurate digital replica of our experimental batch configuration, with a focus on maintaining authentic system dimensions. Our simulation, leveraging ray-tracing, took into account the Fresnel reflection and refraction occurring at the juncture of media with varying refractive indices. This allowed us to ascertain the power incident on the reaction mixture (illustrated in Figure 2a). By integrating this data over the entirety of the receiving surface, the photon flux ($q_{n,p}$) could be determined for all 4 power settings of the light source (Figure 2b).

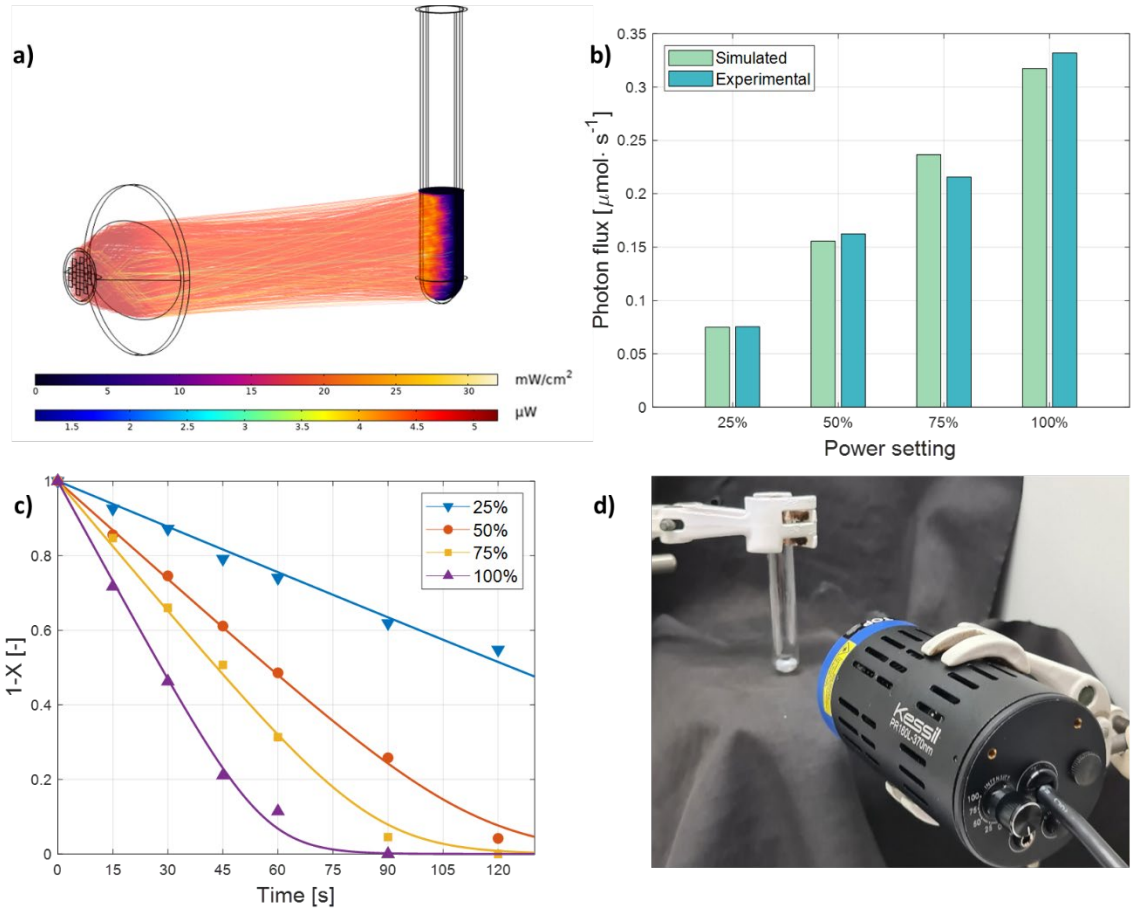

Figure 2. a) The light intensity and a selection of rays (and their energy) reaching the reaction mixture in the batch tube. b) A comparison of the determined photon flux through ray-tracing simulations and fitting using experimental data, for the 4 tested power settings. c) The experimental data and kinetic curves for the investigated batch system, showing the non-converted fraction $1 - X$ of starting material. d) The experimental batch setup, with the lamp positioned 10 cm from the tube. The simulation in a) was done for the 100% power setting (43 W input electrical power), using 24 LEDs with $3 \cdot 10^4$ photons each, $2.4 \cdot 10^4$ of those interacting with the reaction mixture, with only a selection of $1 \cdot 10^3$ of those shown for visualization. For the effective optical path length for the photon flux determination curve in b) and c) the geometric average $\langle l \rangle$ = 10.3 mm from equation (4) was used.

Next, chemical actinometry experiments were carried out for the batch system (see Figure 2d and the Methods section) and the results are presented in Figure 2b and c, which demonstrate excellent agreement between the simulated and actual photon fluxes. To determine the absorbance of the polychromatic light, we employed a modified version of Equation (2), factoring in the lamp's spectral distribution and the wavelength-specific attenuation coefficients. This information facilitated our modeling of the reaction progression over irradiation time, as detailed in the Supplementary Information, resulting in the kinetic curves displayed in Figure 2c. In examining the unreacted reaction mixture, the initial spectrum-average transmittance through the reaction tube is estimated at approximately 0.1% when the inner diameter alone is assumed as the effective optical path length. However, it is crucial to note that not all light will enter the reactor tube through its center, thereby not all light will perceive the inner diameter as the effective path length. Given that the tube is irradiated from a single side, a popular approach for a cylinder is the employment of a geometric average path length.[18] This average can be deduced through integration, or more straightforwardly by visualizing the cylinder as a flat plate, where the total volume is divided by its projected irradiated area (Supplementary Figure S14a):

$$\langle l \rangle = \frac{cylinder\ volume}{projected\ area} = \frac{\pi R^2 H}{2RH} = \frac{\pi R}{2} \approx 1.57R \qquad (4)$$

where $\langle l \rangle$, R and H are the geometric average optical path length, the inner radius and height of the tube, respectively. In our analysis, using the geometric average, we calculated an initial spectrum-average transmittance of ~0.3% - a minuscule value. The negligible difference in transmittance between these two path length measures reveals that the average absorbed fraction ($1 - T$, so 0.999 and 0.997, respectively) is practically independent of the path length. This confirms the nature of this setup as a photon-efficient system, wherein almost the entire photon flux is absorbed. In such a reactor, there is a progressive decline in light intensity, inducing variations in reaction kinetics across the reactor's cross-section. Consequently, the reactor wall experiences high light intensities, potentially leading to over-irradiation and byproduct formation. In contrast, the reactor's center receives no light, preventing reactions from occurring. This indicates that such reactors may not be optimal for conducting photocatalytic transformations. It also underscores that traditional scaling-up approaches, such as dimension enlargement with corresponding larger diameter vessels, are not ideal for photochemical processes.

Lastly, although the exact measurement of the effective optical path length is not a requirement for larger diameter batch apparatus, our methodology (for an overview of the workflow, see Figure S9) underscores the importance of radiometric data collection and three-dimensional modeling as a means to acquire detailed photon flux information. This is evidenced by the remarkable correlation between the experimental outcomes and the simulated data presented in Figure 2b. Such congruence virtually eliminates the necessity of conducting chemical actinometry experiments in systems where intensification is not a factor.

B) Intensified photochemical continuous-flow reactors

To further illustrate the workflow of photon flux determination through radiometry and ray-tracing, we applied the same course of action to two distinct intensified reactor systems. The first system is a well-established microcapillary flow reactor, one of the common lab-scale reactor types that have seen wide applicability due to their operational simplicity, low-cost fabrication, and ease of assembly.[44,45] The second is the high-shear spinning disk reactor,[46] specifically the photo rotor-stator spinning disk reactor (pRS-SDR), a design pioneered by our team.[32,47] Unlike the non-intensified batch reactor, these intensified reactors function in a continuous-flow mode, presenting the potential for scaling up photochemistry. Importantly, the two selected intensified systems vary considerably in their operation, reactor geometry, light source, scale, and reactor-light source configuration, showcasing the versatility of our workflow (for an overview of the workflows, see Figure S10 and S11).

Microcapillary reactor

A custom continuous-flow reactor was assembled using a microcapillary (1.6 mm inner diameter, 3.2 mm outer diameter) coiled around a cylindrical base, which was then placed inside a larger cylindrical chamber. The chamber's inner wall was fitted with an LED strip aligned to irradiate the coiled capillary (Figure 3d). To characterize the light source, light intensity was measured at specified input powers at the chamber's center, with the coiled reactor being absent during the assessment. The LED strip, with its helical design, was then digitally modeled to calibrate the optical input power essential for the photon flux simulations (see Supplementary Information). For the simulations, a three-dimensional digital replica of the coiled capillary tube, mounted on its cylindrical base, was created. This replica was virtually illuminated by the calibrated LED strip through ray-tracing, as illustrated in Figure 3a.

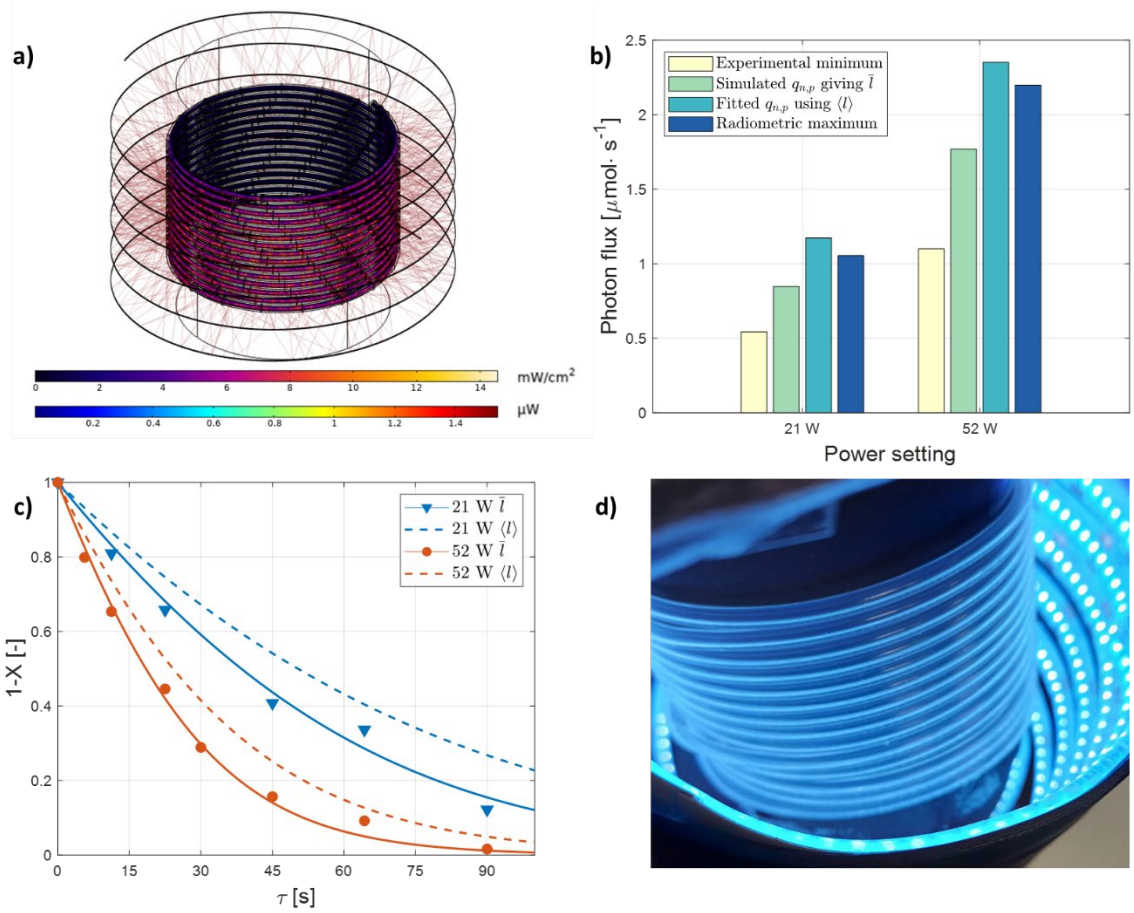

Figure 3. a) The light intensity and a selection of rays (and their energy) reaching the reaction mixture in the coiled capillary reactor. b) A comparison of the determined photon fluxes for the 2 tested power settings. Here, the minimum flux is determined experimentally assuming all light gets absorbed, the maximum flux through the integration of the irradiated surface with the measured radiometric light intensity, the simulated flux through ray-tracing simulations and the fitted flux using the geometric average path length. C) The experimental data and kinetic curves for the investigated capillary reactor system, showing the non-converted fraction $1 - X$ of starting material as a function of residence time τ, for the effective optical path length $\bar{l}$ = 1.85 mm and the geometric average path length $\langle l \rangle$ = 1.25 mm. d) The experimental microcapillary reactor setup, opened and lifted for the picture. The simulation in a) was done for the 52 W power setting (i.e., input electrical power), using 576 LEDs with $2 \cdot 10^3$ photons each, $4.8 \cdot 10^5$ of those interacting with the reaction mixture, with only a selection of $2 \cdot 10^3$ of those shown for visualization.

In our study, the LED strip's input current and resultant potential were adjustable, enabling us to test and simulate two distinct power settings. These simulations revealed received photon fluxes of 0.85 and 1.8 μmol s^{-1} (equivalent to 0.27 and 0.56 W, optical power received by the reaction mixture) for the two settings. We juxtaposed the experimental outcomes with modeled kinetic curves (Figure 3c), produced using the molar balance for the tubular reactor under the assumption of it functioning as an ideal plug flow reactor (see Supplementary Information). In these findings, we differentiate between two path lengths: the effective optical path length, denoted as $\bar{l}$, and the geometric average path length, $\langle l \rangle$, which is defined in Equation (4) for any cylinder irradiated on one side. For the capillary tube, which has an inner diameter of 1.6 mm and an outer diameter of 3.2 mm, the expected geometric average path length is 1.25 mm. This translates to an initial absorbed fraction of roughly 0.53, underlining the significant transmittance. However, the effective optical path lengths determined for this system – which should ideally be consistent across different irradiation powers – stood at 1.9 mm and 1.8 mm for the 21 W and 52 W settings, respectively. These determined effective optical path lengths notably exceed the geometric average path length (i.e., 1.25 mm), leading to a greater initial absorbed fraction of approximately 0.66 and, consequently, a higher conversion rate. As can be seen in Figure 3c, employing the effective optical path length yielded a strong alignment between the simulation and experimental data, whereas utilizing the traditionally adopted geometric average path length led to less accurate

outcomes. Moreover, in light of the radiometric data, the photon fluxes required to attain the optimal kinetic curve fit for a 1.25 mm geometric average path length are unattainable with the current settings of the light source (see Figure 3b).

Several elements might contribute to this unexpected increase in path length. Firstly, the LED strip's inherent non-collimated nature – given its beam angle of around 60° – allows light to enter at varied angles, thereby extending the path length within the medium. Additionally, the tube's curvature and coiling alter the angle at which light hits the air-tube interface, impacting both reflection and, more crucially, refraction. Furthermore, the transparent polymer material of the tube, possessing a refractive index higher than the surrounding air, causes light to refract inward, towards the reaction mixture, effectively lengthening the path.

The inward refraction of incoming light impacts more than just the elongation of the effective optical path length. It also modifies the photon flux received by the reaction mixture. This effect stems from an expanded surface area available for capturing irradiation (see Supplementary Figure S14b and c for details). To illustrate, when the light source's intensity was measured with radiometry, the sensor registered approximately 28 W m^{-2} (i.e., for 21 W input electrical power). However, when the simulated photon flux reaching the reaction mixture at the same distance is assessed over its flat projected irradiated area (as shown in equation (4), $2RH$), the value rises to 45 W m^{-2}. This discrepancy implies that the reactor absorbs far more energy than possible based on the emission of the light source, even after accounting for losses like reflection. This phenomenon arises because the light interacting with the tube's outer surface refracts inward. As a result, the photon collection area for the reactor is determined by the flat projected outer surface, not the inner one. In other words, the light received by the outer area is focused on a smaller reaction medium area, resulting in an inflated value of 45 W m^{-2}. When this adjusted area is used to compute intensity, the resulting effective collected light intensity aligns more accurately at 22 W m^{-2}.

Subsequent experiments with doubled and quadrupled actinometer concentrations were conducted to underscore the importance of accurate path length determination in low-transmittance systems (see Supplementary Figure S12b). With elevated concentrations, the absorption characteristics (εC) of the reaction mixture became predominant, shifting the initial reactor conditions towards photon-efficient behavior characterized by almost complete absorption of the light.

In another set of experiments, we explored the potential impact of the cylindrical capillary holder's surface. While previous experiments utilized a non-refractive black surface for this cylinder, optimizing energy utilization could involve making this surface reflective to increase photon absorption. This enhancement would manifest in two primary ways: firstly, by amplifying the received flux, and secondly, by extending the effective path length of the previously received irradiation. The enhanced flux would arise from initially missed irradiation being reflected back towards the capillary, offering another opportunity for interaction with the absorbing medium. In contrast, the extended path length would come from transmitted irradiation – already passed through the reaction mixture – being reflected for another pass. Simulations with a reflective supporting cylinder, assuming lossless specular reflection, indeed showed an increase in total received photon fluxes for both power settings, reaching 1.0 and 2.2 µmol s^{-1} (equivalent to 0.33 and 0.69 W optical power received by the reaction mixture), representing a 22% boost of the photon flux due to the reflective material. When combining these fluxes with experimental data, the effective optical path length extended to approximately ~2.3 mm (see Supplementary Figure S12a).

Photo rotor-stator spinning disk reactor (pRS-SDR)

The subsequent reactor analyzed was the intensified continuous pRS-SDR. This setup incorporated the reactor and an LED-based floodlight, both housed within a stainless steel casing (Figure 4d).[32,47] The reactor's design features a fast rotating disk (the rotor) encased in narrow-fitting housing, called the stator. The stator is strategically placed 2 mm away from the rotor, resulting in a multifaceted geometry with several reflective, non-transparent stainless-steel components. The irradiation process is facilitated through a quartz window, serving as the upper stator. Comprehensive characterization of the floodlight was undertaken, which was then integrated into a detailed model of the entire assembly, as depicted in Figure 4a.

The floodlight was designed to function at a singular power setting. Therefore, both the experiments and simulations adhered to this specific power input, resulting in a simulated photon flux received of 12.5 µmol s^{-1} (~4.1 W optical power received by the reaction mixture). Figure 4c showcases the kinetic curves at different rotor rotation speeds, along with their corresponding fits. Unlike the microcapillary reactor, the molar balance for the pRS-SDR was developed under the presumption that the reactor emulates the behavior of a continuously stirred tank reactor (CSTR). This presumption is grounded in our previous studies which indicate that CSTR behavior prevails under standard pRS-SDR operation (Supplementary Information).[48,49] From the experimental data, it is evident that the rotor's rotation speed has a minimal impact on the reaction rate. This suggests that the system operates not in a mass-transfer limited domain, but predominantly within a photon-limited regime. The projected geometric average path length for this reactor was estimated at the axial gap distance (i.e., the spacing between the quartz stator and rotor), which is 2.0 mm. Based on this value, an initial photon absorption rate of approximately ~0.78 can be derived.

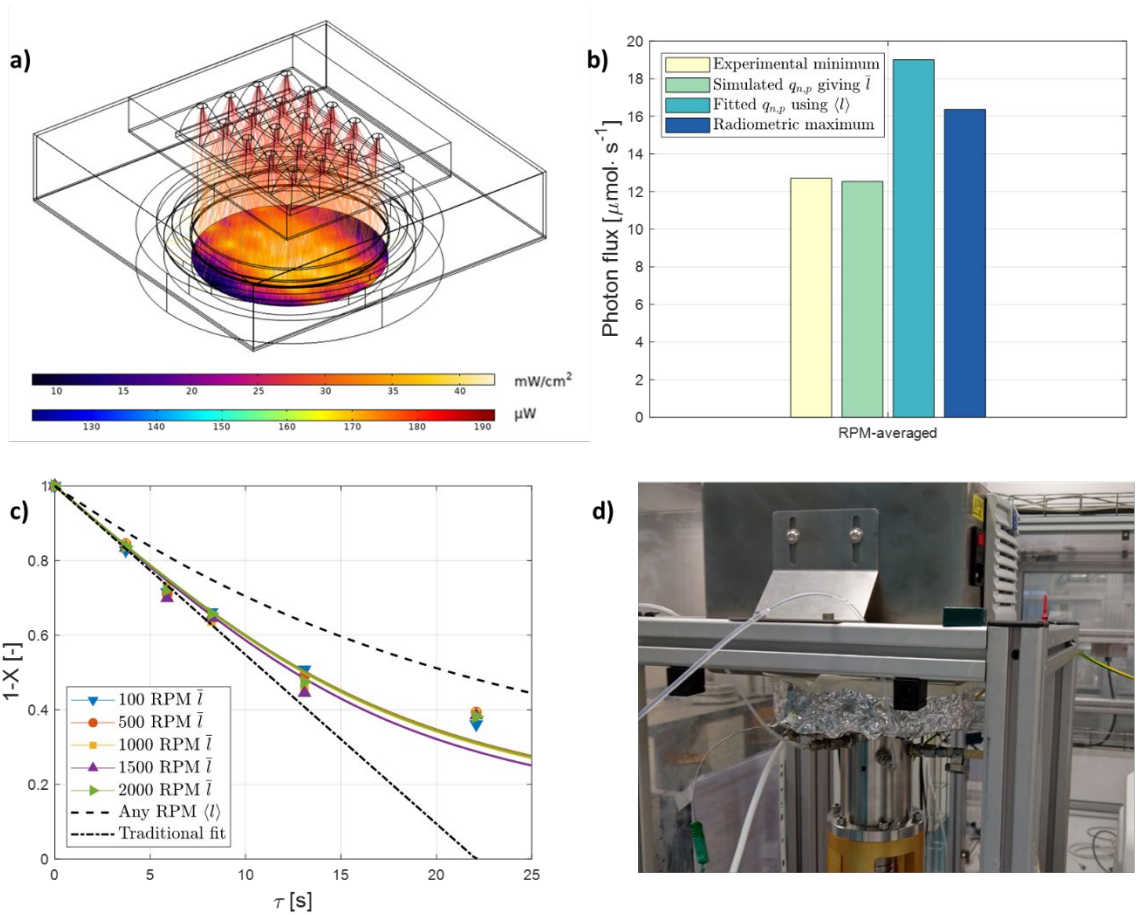

Figure 4. a) The light intensity and a selection of rays (and their energy) reaching the reaction mixture in pRS-SDR. b) A comparison of the determined photon fluxes for the pRS-SDR. Here, the minimum flux is determined experimentally assuming

all light gets absorbed, the maximum flux through integration of the radiometric intensity, the simulated flux through ray-tracing simulations, and the fitted flux using the geometric average path length. C) The experimental data and kinetic curves for the investigated pRS-SDR system, showing the non-converted fraction $1 - X$ *of starting material as a function of residence time* τ*, for their effective optical path lengths (average of* $\bar{l}$ *= 5.3 mm) and the geometric average path length* $\langle l \rangle$ *= 2.0 mm. d) The experimental pRS-SDR setup. The simulation in a) was done for a power input of 175 W, using 20 LEDs with* $1.5 \cdot 10^3$ *photons each,* $2.4 \cdot 10^4$ *of those interacting with the reaction mixture, with only a selection of* $1 \cdot 10^3$ *of those shown for visualization.*

The effective optical path length, however, was found to be 5.3 ± 0.2 mm, notably larger than the geometric average path length of 2.0 mm. Employing this effective optical path length, an initial absorbed photon fraction of ~0.98 can be derived, intrinsically resulting from the close agreement between the experimentally determined minimum and simulated photon flux (Figure 4b). Absorption of the majority of photons gives a markedly enhanced conversion rate and, in comparison to the microcapillary reactor (Figure 3b), a lower fraction of photons transmitted. This further underscores the criticality of basing conclusions on accurate presumptions when interpreting data.

Intriguingly, significant chemical conversions – typically observed at prolonged residence times – are essential to discern the notable impact of path length variations. This phenomenon is evident in the initial gradient of the kinetic curves depicted in Figure 4c. At such low conversions, the disparity between different path lengths seems minimal. However, as conversion increases, the curves noticeably diverge, with the effective optical path length playing an increasingly dominant role in the kinetics and the accuracy of the models. Using conventional photon flux determination methods, which assume complete absorption of the incident light, and fitting a linear model to the initial gradient (the traditional fit in Figure 4c), an average received photon flux of 12.7 µmol s^{-1} (~4.1 W optical power received by the reaction mixture) is found. This contrasts only marginally with the flux determined via radiometry and ray-tracing, which was less than 2% lower. Interestingly, if one were to apply the known gap distance of 2.0 mm, the needed received photon flux approximates ~19.0 µmol s^{-1} (~6.2 W optical power received by the reaction mixture). This value exceeds the total optical output power of the floodlight (~5.3 W optical power emitted by the light source) as determined with radiometry and ray-tracing, rendering this as an implausible outcome (all discussed fluxes are shown in Figure 4b).

Several factors could account for the evident discrepancy between the anticipated and fitted path lengths. The light source's beam angle affects the angle of incidence and, in turn, the initial single-pass path length. Additionally, the rotor might reflect light diffusely back into the system, allowing for a second pass. Another factor to consider is the phenomenon of total internal reflection, stemming from the pronounced refractive index difference at the quartz-air interface, which can confine a portion of the photons within the system. Given the knowledge that the initial transmittance following the determined 5.3 mm effective optical path length is virtually negligible, categorizing this reactor as a photon-efficient system becomes unexpectedly justified (Figure S15). This highlights that the significance of accurate path length determination is intimately tied to the dimensions, and the absorbing attributes of the medium.

Conclusion and outlook

In this study, we present a comprehensive workflow to ascertain the photon flux and effective optical path length for intensified photoreactors. Recognizing that the effective optical path length in intricate photochemical reactors and setups is challenging to define with a single predetermined value, we proposed its determination through a synergistic approach involving radiometry, ray-tracing, and chemical actinometry. Instead of relying solely on manufacturer-provided optical output data, we conduct radiometric measurements to quantify light intensity across multiple distinct points, factoring in potential light source decay. This information serves as a calibration benchmark for virtual light source simulations. Ray-tracing emerges as an invaluable instrument, granting profound insights into light sources and photoreactors.[15,50] Our modeling approach, though necessitating precise light source

and reactor representations, proves adept at handling even reactors with complex geometries and non-trivial effective optical path lengths, such as those incorporating static mixers or featuring non-transparent backplates. Only a description of the reactor's outer surface and reactor-medium interface suffices for determining the received photon flux, thereby obviating intricate photon path assessments within ray-tracing software.

The outcome of our ray-tracing simulations and experimental endeavors aims to shed light on irradiation profiles and photon absorption, offering predictive capabilities for absorption properties across diverse photochemical systems. Additionally, by integrating the unique geometry of different reactor designs, photon fluxes and effective path lengths can be ascertained through data fitting from a single kinetic experimental curve. Our methodology underwent rigorous validation using a non-intensified batch reactor, and its application extended to determining photon flux and effective optical path length in both a microflow and a photo rotor-stator spinning disk reactor. Intriguingly, the effective optical path length derived did not mirror the results obtained by using the frequently applied geometric average path length, underscoring the pivotal roles played by factors like diffuse emission, reflection, and refraction. Indeed, resorting to geometric average path lengths when deducing photon flux could yield results that defy physical possibility, given the constraints of the light sources and radiometric data at hand. This revelation underscores the paramount importance of accurately obtaining effective optical path lengths and attests to the robustness of our proposed workflow.

While our method has been exemplified through the widely used ferrioxalate actinometer in intensified reactors, its applicability spans other chemical actinometers across varied configurations. Essential prerequisites include knowledge of the actinometer's absorption data and its products, as well as the light source's spectral distribution. Moreover, meticulous detailing of the geometries of the light source, light sensor, and photoreactor facilitates a representative portrayal within streamlined ray-tracing simulations.

We are confident that our innovative workflow will offer invaluable insights into photochemical reactor designs, serving as an essential tool for process engineers in the industry. Not only does it hold the potential to significantly enhance energy balance evaluations, but it also stands as a pivotal asset for conducting Operational Expenditure (OPEX) assessments by facilitating foresight in anticipating and optimizing material usage. Furthermore, the workflow leads to efficient scale-up studies, by enabling straightforward characterization and design of systems. By bridging the gap between theoretical understanding and practical application, we anticipate our methodology will drive advancements in photochemical reactor optimization and contribute meaningfully to sustainable chemical processing.

Methods

Chemical actinometry

Potassium ferrioxalate has been used as chemical actinometer, and the experimental procedure was based on literature.[11,51] The potassium ferrioxalate was either directly used from the supplier (Alfa Aesar) or made by mixing iron(III)chloride (Sigma Aldrich) with di-potassium oxalate (Sigma Aldrich) in a 1:3 mole ratio. The product was obtained by crystallization, which was performed two times, whereafter the crystals were placed in a desiccator to dry.

A solution of 6 mM of potassium ferrioxalate in 50 mM sulfuric acid (Sigma Aldrich) solution, using demineralized water as solvent, was prepared. The solution was loaded in the batch reactor or pumped through the microcapillary/photo rotor-stator spinning disk reactor (pRS-SDR), under the irradiation of UV-light source (Batch reactor: Kessil PR160L 370 nm, input power 43 W; microcapillary reactor: LuxaLight UV-A 365 nm LED strip, input power 52 W; pRS-SDR: UV-A curing 365 nm floodlight,

input power 175 W). The reactor was placed at a known position relative to the light source. The batch test tube (Pyrex, inner diameter 13.2 mm, outer diameter 15.2 mm, filled with 4 mL reaction mixture) was stirred, using a magnetic stirrer and stirrer bar. This tube was removed after the set irradiation time, whereafter a sample was taken. A new unirradiated tube was used to obtain the subsequent data point to ensure that the volume inside the reactor remained constant. For the continuous reactor types, samples were taken at the outlet after waiting several residence times to ensure steady-state conditions. The microcapillary reactor (PFA, 1.6 mm inner diameter, 3.2 mm outer diameter, 7.5 mL) was operated in continuous mode rather than using stop-flow, due to increased mixing and prevention of unwanted dilution.[12,52] For the pRS-SDR the total volume was used to express the residence time (59 mL excluding connections, ~28 mL irradiated volume). All experiments and the preparation of the solutions and samples were conducted in a darkroom.

The samples (0.1 mL) were diluted with water (1.4 mL) and after dilution 0.6 mL was added to a buffer solution (2.0 mL). The buffer consisted of 6 mM 1,10-phenanthroline (Sigma Aldrich), 0.6 M sodium acetate (Sigma Aldrich) in 0.18 M sulfuric acid, using demineralized water as solvent. The samples were measured using a UV-VIS Spectrophotometer (UV-2501 PC, Shimadzu) in a 1 cm quartz cuvette at the absorption peak of the formed complex found at 510 nm.

Radiometry

Radiometric characterization of the light sources was done with a UV light sensor (RM12 Sensor Opsytec Dr. Göbel UVA+), that could be placed at a known position relative to the light source, in a predefined grid. After the fixation of the sensor, proper shielding of the environment was ensured, whereafter the light source was turned on. The light intensity after stabilization of the value was noted. A dark experiment was conducted to account for any possible background irradiation.

Ray-tracing

For the development of the light source and reactor setup simulations, geometric representations of the light sources and reactors were made based on the measured dimensions. These representations, including material properties, were modeled in COMSOL Multiphysics 5.4. For the radiometric ray-tracing calibration, the UV sensor used for the experimental data was recreated as well. The simulations were conducted using the Geometric Optics module with the time-dependent solver, with time-stepping calculated with the generalized alpha algorithm. Moreover, the solution of the linear system of equations proceeded iteratively with the GMRES method. Here the relevant release information (direction vector, emission profile, ray properties, and total power) could be defined. The irradiated surface (either the sensor or reaction mixture) was defined as an accumulator that freezes the incident ray and deposits the ray's power onto the surface. This allowed us to obtain the optical output power of the light source, through calibration of the virtual received intensities to the experimental quantities, as well as estimate the emission profile at the same time (e.g., Lambertian, conical, or hemispherical emission), by minimizing the error in intensity distribution differences. Both mesh dependency and result convergence studies as a result of simulation size have been done (see Supplementary Information).

Non-linear fitting of effective optical path length

The kinetic curves' molar balances (Supplementary Information) were implemented in MATLAB R2022b. A non-linear least squares method was used to fit the effective optical path length (or photon flux for the batch system) in the balance. The differential equations were solved with a variable-step, variable-order (VSVO) solver for stiff differential equations.

Acknowledgements

We want to express our gratitude to the molecular photonics group (Van 't Hoff Institute for Molecular Sciences, University of Amsterdam) for using the darkroom and to Dr. M.G. Debije (Eindhoven University of Technology) for his assistance with the radiometric measurements. S.D.A.Z., J.H.A.S.,

and T.N. would like to thank the European Union's Horizon research and innovation program FlowPhotoChem (S.D.A.Z. and T.N.), grant number 862453 and CATART (J.H.A.S. and T.N.), grant agreement number 101046836). A.C. would like to thank Janssen Pharmaceutica NV for research funding. C.S. and N.P. would like to thank the Coordination for the Improvement of Higher Education Personnel (CAPES, Brazil, grant number 88887.310560/2018-00) and the National Council for Scientific and Technological Development (CNPq, Brazil, grant number 313202/2021-4 and 312247/2022-2) for funding. The materials presented and views expressed here are the responsibility of the authors(s) only. The EU Commission takes no responsibility for any use made of the information set out.

References

1. Marzo, L., Pagire, S. K., Reiser, O. & König, B. Visible-Light Photocatalysis: Does It Make a Difference in Organic Synthesis? *Angew. Chemie Int. Ed.* **57**, 10034–10072 (2018).

2. Ravelli, D., Dondi, D., Fagnoni, M. & Albini, A. Photocatalysis. A multi-faceted concept for green chemistry. *Chem. Soc. Rev.* **38**, 1999 (2009).

3. Liu, J., Lu, L., Wood, D. & Lin, S. New Redox Strategies in Organic Synthesis by Means of Electrochemistry and Photochemistry. *ACS Cent. Sci.* **6**, 1317–1340 (2020).

4. Crisenza, G. E. M. & Melchiorre, P. Chemistry glows green with photoredox catalysis. *Nat. Commun.* **11**, 803 (2020).

5. Donnelly, K. & Baumann, M. Scalability of photochemical reactions in continuous flow mode. *J. Flow Chem.* **11**, 223–241 (2021).

6. Buglioni, L., Raymenants, F., Slattery, A., Zondag, S. D. A. & Noël, T. Technological Innovations in Photochemistry for Organic Synthesis: Flow Chemistry, High-Throughput Experimentation, Scale-up, and Photoelectrochemistry. *Chem. Rev.* **122**, 2752–2906 (2022).

7. Zondag, S. D. A., Mazzarella, D. & Noël, T. Scale-Up of Photochemical Reactions: Transitioning from Lab Scale to Industrial Production. *Annu. Rev. Chem. Biomol. Eng.* **14**, 283–300 (2023).

8. Corcoran, E. B., McMullen, J. P., Lévesque, F., Wismer, M. K. & Naber, J. R. Photon Equivalents as a Parameter for Scaling Photoredox Reactions in Flow: Translation of Photocatalytic C−N Cross-Coupling from Lab Scale to Multikilogram Scale. *Angew. Chemie - Int. Ed.* **59**, 11964–11968 (2020).

9. Su, Y., Straathof, N. J. W., Hessel, V. & Noël, T. Photochemical Transformations Accelerated in Continuous-Flow Reactors: Basic Concepts and Applications. *Chem. – A Eur. J.* **20**, 10562–10589 (2014).

10. Wong, K.-L., Bünzli, J.-C. G. & Tanner, P. A. Quantum yield and brightness. *J. Lumin.* **224**, 117256 (2020).

11. Hatchard, C. G. & Parker, C. A. A new sensitive chemical actinometer - II. Potassium ferrioxalate as a standard chemical actinometer. *Proc. R. Soc. London. Ser. A. Math. Phys. Sci.* **235**, 518–536 (1956).

12. Wriedt, B. & Ziegenbalg, D. Common pitfalls in chemical actinometry. *J. Flow Chem.* **10**, 295–306 (2020).

13. Radjagobalou, R. *et al.* A revised 1D equivalent model for the determination of incident photon flux density in a continuous-flow LED-driven spiral-shaped microreactor using the actinometry method with Reinecke's salt. *J. Flow Chem.* **11**, 357–367 (2021).

14. Cambié, D., Zhao, F., Hessel, V., Debije, M. G. & Noël, T. Every photon counts: Understanding and optimizing photon paths in luminescent solar concentrator-based photomicroreactors (LSC-

PMs). *React. Chem. Eng.* **2**, 561–566 (2017).

15. Kant, P. *et al.* Isophotonic reactor for the precise determination of quantum yields in gas, liquid, and multi-phase photoreactions. *Chem. Eng. J.* **452**, 139204 (2023).

16. de Oliveira, G. X., Kuhn, S., Riella, H. G., Soares, C. & Padoin, N. Combining computational fluid dynamics, photon fate simulation and machine learning to optimize continuous-flow photocatalytic systems. *React. Chem. Eng.* **8**, 2119–2133 (2023).

17. Noël, T. *Photochemical Processes in Continuous-Flow Reactors*. (WORLD SCIENTIFIC (EUROPE), 2017). doi:10.1142/q0065.

18. Roibu, A. *et al.* An accessible visible-light actinometer for the determination of photon flux and optical pathlength in flow photo microreactors. *Sci. Rep.* **8**, (2018).

19. Megerle, U., Lechner, R., König, B. & Riedle, E. Laboratory apparatus for the accurate, facile and rapid determination of visible light photoreaction quantum yields. *Photochem. Photobiol. Sci.* **9**, 1400–1406 (2010).

20. Cismesia, M. A. & Yoon, T. P. Characterizing chain processes in visible light photoredox catalysis. *Chem. Sci.* **6**, 5426–5434 (2015).

21. Scaiano, J. C. A beginners guide to understanding the mechanisms of photochemical reactions: things you should know if light is one of your reagents. *Chem. Soc. Rev.* **52**, 6330–6343 (2023).

22. Swierk, J. R. The Cost of Quantum Yield. *Org. Process Res. Dev.* **27**, 1411–1419 (2023).

23. Braslavsky, S. E. *et al.* Glossary of terms used in photocatalysis and radiation catalysis (IUPAC recommendations 2011). *Pure Appl. Chem.* **83**, 931–1014 (2011).

24. Noël, T. & Zysman-Colman, E. The promise and pitfalls of photocatalysis for organic synthesis. *Chem Catal.* **2**, 468–476 (2022).

25. Maafi, M. & Brown, R. G. The kinetic model for AB(1ϕ) systems. *J. Photochem. Photobiol. A Chem.* **187**, 319–324 (2007).

26. Sambiagio, C. & Noël, T. Flow Photochemistry: Shine Some Light on Those Tubes! *Trends Chem.* **2**, 92–106 (2020).

27. Williams, J. D. & Kappe, C. O. Recent advances toward sustainable flow photochemistry. *Curr. Opin. Green Sustain. Chem.* **25**, 100351 (2020).

28. Loubière, K., Oelgemöller, M., Aillet, T., Dechy-Cabaret, O. & Prat, L. Continuous-flow photochemistry: A need for chemical engineering. *Chem. Eng. Process. Process Intensif.* **104**, 120–132 (2016).

29. De Risi, C. *et al.* Recent advances in continuous-flow organocatalysis for process intensification. *React. Chem. Eng.* **5**, 1017–1052 (2020).

30. Russo, D. *et al.* Direct photolysis of benzoylecgonine under UV irradiation at 254nm in a continuous flow microcapillary array photoreactor. *Chem. Eng. J.* **283**, 243–250 (2016).

31. Lee, D. S. *et al.* Scalable Continuous Vortex Reactor for Gram to Kilo Scale for UV and Visible Photochemistry. *Org. Process Res. Dev.* **24**, 201–206 (2020).

32. Chaudhuri, A. *et al.* Process intensification of a photochemical oxidation reaction using a Rotor-Stator Spinning Disk Reactor: A strategy for scale up. *Chem. Eng. J.* **400**, 125875 (2020).

33. Wen, Z. *et al.* Optimization of a Decatungstate-Catalyzed C(sp 3)–H Alkylation Using a Continuous Oscillatory Millistructured Photoreactor. *Org. Process Res. Dev.* **24**, 2356–2361 (2020).

34. Wan, T. *et al.* Accelerated and Scalable C(sp 3)–H Amination via Decatungstate Photocatalysis Using a Flow Photoreactor Equipped with High-Intensity LEDs. *ACS Cent. Sci.* **8**, 51–56 (2022).

35. Wriedt, B., Kowalczyk, D. & Ziegenbalg, D. Experimental Determination of Photon Fluxes in Multilayer Capillary Photoreactors. *ChemPhotoChem* **2**, 913–921 (2018).

36. Vandekerckhove, B., Piens, N., Metten, B., Stevens, C. V. & Heugebaert, T. S. A. Practical Ferrioxalate Actinometry for the Determination of Photon Fluxes in Production-Oriented Photoflow Reactors. *Org. Process Res. Dev.* **26**, 2392–2402 (2022).

37. Roibu, A., Mc Carogher, K., Morthala, R. B., Eyckens, R. & Kuhn, S. Modelling approaches to predict light absorption in gas-liquid flow photosensitized oxidations. *Chem. Eng. J.* **452**, 139272 (2023).

38. Cornet, J.-F. *et al.* A Simple and Reliable Method to Determine Mean Incident Light Flux Densities on Cylindrical Photoreactors and Photobioreactors from a Unique Fluence Rate Measurement. *Ind. Eng. Chem. Res.* **62**, 4875–4884 (2023).

39. Yaghmaei, M. & Scaiano, J. C. A simple Norrish Type II actinometer for flow photoreactions. *Photochem. Photobiol. Sci. 2023* **1**, 1–10 (2023).

40. Aillet, T., Loubiere, K., Dechy-Cabaret, O. & Prat, L. Accurate measurement of the photon flux received inside two continuous flow microphotoreactors by actinometry. *Int. J. Chem. React. Eng.* **12**, 257–269 (2014).

41. Shin, N. Y., Ryss, J. M., Zhang, X., Miller, S. J. & Knowles, R. R. Light - driven deracemization enabled by excited - state electron transfer. *Science.* **366**, 364–369 (2019).

42. Hu, H. *et al.* Metal–organic frameworks embedded in a liposome facilitate overall photocatalytic water splitting. *Nat. Chem.* **13**, 358–366 (2021).

43. Rabani, J., Mamane, H., Pousty, D. & Bolton, J. R. Invited Review Practical Chemical Actinometry-A Review. *Photochem. Photobiol.* **97**, 873–902 (2021).

44. Plutschack, M. B., Pieber, B., Gilmore, K. & Seeberger, P. H. The Hitchhiker's Guide to Flow Chemistry. *Chem. Rev.* **117**, 11796–11893 (2017).

45. Neyt, N. C. & Riley, D. L. Application of reactor engineering concepts in continuous flow chemistry: a review. *React. Chem. Eng.* **6**, 1295–1326 (2021).

46. Chaudhuri, A. *et al.* Kinetics and intensification of tertiary amine N-oxidation: Towards a solventless, continuous and sustainable process. *Chem. Eng. J.* **416**, 128962 (2021).

47. Chaudhuri, A., Zondag, S. D. A., Schuurmans, J. H. A., van der Schaaf, J. & Noël, T. Scale-Up of a Heterogeneous Photocatalytic Degradation Using a Photochemical Rotor–Stator Spinning Disk Reactor. *Org. Process Res. Dev.* **26**, 1279–1288 (2022).

48. de Beer, M. M., Keurentjes, J. T. F., Schouten, J. C. & Van der Schaaf, J. Engineering model for single-phase flow in a multi-stage rotor–stator spinning disc reactor. *Chem. Eng. J.* **242**, 53–61 (2014).

49. de Beer, M. M., Pezzi Martins Loane, L., Keurentjes, J. T. F., Schouten, J. C. & van der Schaaf, J. Single phase fluid-stator heat transfer in a rotor–stator spinning disc reactor. *Chem. Eng. Sci.* **119**, 88–98 (2014).

50. Rochatte, V. *et al.* Radiative transfer approach using Monte Carlo Method for actinometry in complex geometry and its application to Reinecke salt photodissociation within innovative pilot-scale photo(bio)reactors. *Chem. Eng. J.* **308**, 940–953 (2017).

51. Kuhn, H. J., Braslavsky, S. E. & Schmidt, R. Chemical actinometry (IUPAC Technical Report). *Pure Appl. Chem.* **76**, 2105–2146 (2004).

52. Wriedt, B. & Ziegenbalg, D. Application Limits of the Ferrioxalate Actinometer. *ChemPhotoChem* **5**, 947–956 (2021).